

## Crustal Poisson's Ratio Off Eastern Taiwan From OBS Data Modeling

Tan K. Wang<sup>1,\*</sup> and Chi Hua Pan<sup>1</sup>

(Manuscript received 30 September 2000, in final form 1 February 2001)

### ABSTRACT

One vertical component and two horizontal components of 27 ocean-bottom seismometer (OBS) data sets along four profiles off eastern Taiwan were obtained using a large air-gun array of the R/V Maurice Ewing during summer/fall 1995. From the horizontal components of the OBS data, we identify most refractions converted in the sediment and reflections converted in the crust respectively as the first and later arrivals. These converted arrivals are subsequently used for travel-time modeling of the sedimentary and crustal Poisson's ratios. The overall results show differences of Poisson's ratios in the accretionary prism (0.28~0.3), the continental crust (0.25~0.29) and the oceanic slab (0.23~0.33), and these are associated with the different structural compositions and/or tectonic settings. OBS data modeling of profile EW9509-1, which covers the Ryukyu arc-trench system in the north-south direction, reveals relatively low Poisson's ratios in the northern portion of the Yaeyama accretionary prism (0.28) and in the southern portion of the Ryukyu Arc basement (0.25). Anomalous Poisson's ratios within the accretionary prism and the continental crust may be attributed to the fractures of the forearc compression beneath the Nanao Basin. From the east-west profiles of EW9509-14 and EW9509-16 across three forearc basins, we also find anomalously high Poisson's ratios (0.27~0.29) for the Ryukyu Arc basement beneath the Nanao Basin. High Poisson's ratios of the overlying plate suggest the presence of fluid-filled micro-cracks, which may be related to the northward movement of the Luzon Arc and the Gauga Ridge. Poisson's ratio decreases northwestward along profile EW9509-23 that is consistent with the increasing crustal thickness northwestward in the P-wave modeling below the Huatung Basin.

(Key words: OBS, Poisson's ratio, Shear wave, Converted wave)

---

<sup>1</sup>Institute of Applied Geophysics, National Taiwan Ocean University, Keelung, Taiwan, ROC

\* *Corresponding author address:* Dr. Tan K. Wang, Institute of Applied Geophysics, National Taiwan Ocean University, Keelung 20224, Taiwan, ROC

E-mail: tkwang@mail.ntou.edu.tw

## 1. INTRODUCTION

The complexity of sedimentary and crustal structures off eastern Taiwan has been attributed to the oblique convergence of the Philippine Sea Plate (PSP) and the Eurasian Plate (EP), as illustrated by the tectonic provinces and the sea floor in Fig. 1. Off northeastern Taiwan, the northward subduction of the PSP beneath the Ryukyu Arc and the southward extension of the Okinawa Trough led to the forearc compression of the Ryukyu Arc basement and the northern Yaeyama accretionary prism (Wang et al. 2001). Off southeastern Taiwan, the northwestward collision of the Luzon Arc and the EP continent generated the collision front along the east coast, whereas the northward subduction of the Gagua Ridge (Schnurle et al. 1998) resulted in the fracture zones beneath the Huatung Basin (Kao et al. 2000). Understanding the sedimentary and crustal properties off eastern Taiwan is critical. For example, relocations and mechanisms of earthquakes in this seismogenic zone can be enhanced on the basis of velocity models of P- and S-waves.

Various geophysical properties have been investigated to understand the complexity of the sedimentation and the crustal structures off eastern Taiwan. Among them, P-wave velocities from deep seismic acquisitions (Hagen et al. 1988; Cheng et al. 1996) and from earthquake tomography (Hsu 2001) have been derived to image the crust with higher resolution than gravity and magnetism. However, due to limitations with respect to instrumentation and data quality in the marine environment, these P-wave velocity models have neither delineated the specific boundaries of the tectonic structures nor determined the structural composition.

On the other hand, the Poisson's ratio (or the ratio of S-wave velocity over P-wave velocity) of the various tectonic structures can be used to identify the structural composition, fracture and fluid saturation, including gas hydrates (Tinivella and Accaino 2000). The reasons for using anomalous Poisson's ratio to investigate the lithosphere are numerous. The Poisson's ratio of the continental crust or a crust older than 140 Ma is generally uniform and less than 0.28 (Holbrook et al. 1988) compared with the irregular and highly variable Poisson's ratio of the young oceanic crust. Shaw (1994) and Kodaira et al. (1996) indicated that the Poisson's ratio of an oceanic crust less than 15Ma can reach the highest value of 0.33. On the other hand, due to variations in structural composition and porosity, the Poisson's ratio of an oceanic crust can vary from 0.25 to 0.32 (Bratt and Solomon 1984; Christensen 1996). Since most oceanic sediments are less consolidated, their Poisson's ratios might be as high as 0.39~0.49 (Iwasaki et al. 1994; Christeson et al. 1997). Hence, models of the Poisson's ratio in this study can be used to understand the structural compositions and the tectonic settings of the lithosphere off eastern Taiwan. On the basis of travel-time modeling and fractured models, Shaw (1994) proposed an anomalously low Poisson's ratio (0.24) for highly fractured crusts but high Poisson's ratios (0.28~0.3) for less fractured crusts. Alternatively, high Poisson's ratio and S-wave anisotropy were evidence of fluid-filled micro-cracks (Mjelde et al. 1995). It is followed that highly fractured rocks and/or pore fluids resulting from the subduction and the arc-continent collision off eastern Taiwan can be identified from the anomalous Poisson's ratios in this study. The aim of this paper is to investigate these anomalous Poisson's ratios enclosed by the well-constrained interfaces for confirming tectonic boundaries and for identifying fracture zones

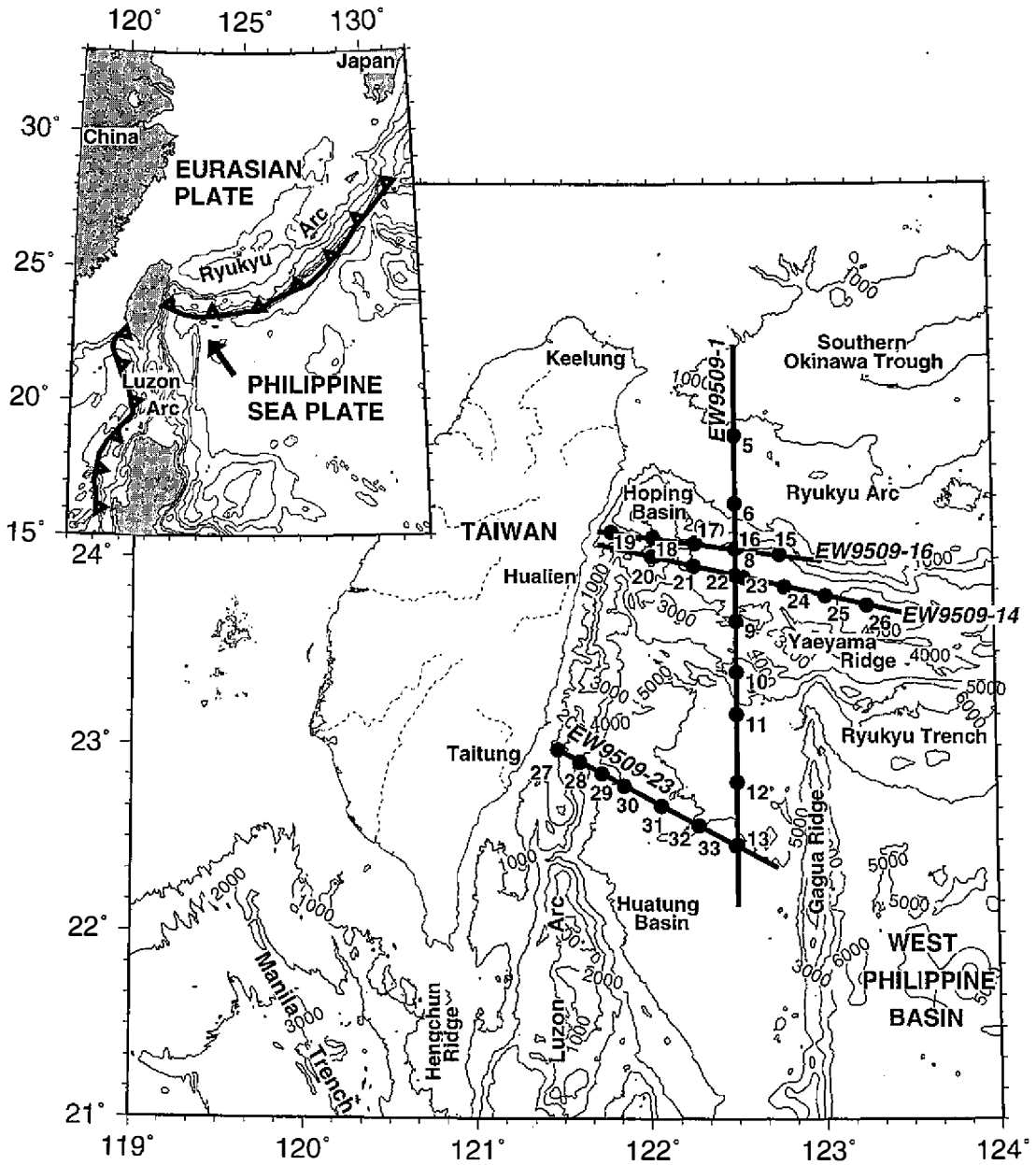


Fig. 1. Bathymetry, tectonic features and locations of the four OBS/MCS lines, namely EW9509-1, EW9509-14, EW9509-16 and EW9509-23, off eastern Taiwan. Solid circles indicate the location of the 27 OBS stations in the experiment. Contour interval of the bathymetry is 1,000 meters.

and fluid intrusions in the Ryukyu arc-trench system and in the Huatung Basin.

## 2. P-WAVE VELOCITY PROFILES FROM OBS DATA MODELING

In August and September 1995, twenty-seven ocean-bottom seismometers (OBS) deployed by the R/V Ocean Researcher I and four corresponding multi-channel seismic (MCS) lines collected by the R/V Maurice Ewing (Fig. 1) were implemented off eastern Taiwan (Liu et al. 1997). OBS and MCS data modeling of four P-wave velocity ( $V_p$ ) profiles (McIntosh and Nakamura 1998; Wang and Chiang 1998; Yang and Wang 1998; Wang et al. 2001) provided velocity and interface information of crustal structures with the highest resolution ever achieved in this region. The P-wave velocity of profile EW9509-1 (Wang et al. 2001) shows a suddenly decreasing thickness (from 7.5 km to 6 km) and an abruptly increasing angle (from 5 degrees to 25 degrees) of the subduction slab ( $V_p = 6.75\sim 7.75$  km/sec) below the Nanao Basin. A southward dipping interface ( $V_p$  contour of 6.75 km/sec) of about 30 degrees within the Ryukyu Arc and the variation of the Moho ( $V_p$  contour of 7.75 km/sec) beneath the Ryukyu Arc may have resulted from the northward subduction of the PSP. The thickness of the Ryukyu Arc basement ( $V_p = 5.5\sim 6.75$  km/sec) and the subducting PSP crust ( $V_p = 6.75\sim 7.75$  km/sec) along two profiles, i.e., EW9509-14 (McIntosh and Nakamura 1998) and EW9509-16 (Wang and Chiang 1998), are 10~15 km and 8~12 km, respectively. The old sediment ( $V_p = 3\sim 4.5$  km/sec) and the upper crust ( $V_p = 4.5\sim 5.5$  km/sec) beneath the Hopping Basin is thickening westward, which may be attributed to either the westward convergence of the PSP or the collision of the Luzon Arc and the Ryukyu Arc. The thickness of the oceanic layer ( $V_p = 4.5\sim 7.75$  km/sec) southeast of OBS 31 in the EW9509-23 profile (Yang and Wang 1998) is 5~7 km, whereas the crust northwest of OBS 31 is thickening northwestward. The velocity variation of the sediment and the upper crust below OBS stations 27 and 28 imply that the eastern boundary of the Luzon Arc is between stations 28 and 29. Low velocity zones in the sedimentary layers and in the upper crust ( $V_p < 7$  km/sec) are easily identified below OBS stations 30, 32 and 33.

The P-wave velocity profiles introduced above as well as the horizontal components of the OBS data acquired in the 1995 experiment have previously been used to construct the Poisson's ratios of three OBS profiles (EW9509-1, EW9509-16 and EW9509-23). Preliminary profiles of the Poisson's ratios were proposed by Wang (1997) and Wang et al. (1998) elsewhere to investigate fracture zones of the tectonic motions off eastern Taiwan. However, due to the inadequate constraints on their structural interfaces, those earlier results failed to determine the specific boundaries of the fracture zones. In this study, the converted boundaries of the shear waves can be properly evaluated from the well-constrained interfaces of four P-wave velocity profiles. Reliable Poisson's ratios are thus obtained in this way and are used to identify fractures and porosities of various tectonic structures off eastern Taiwan.

## 3. PHASE IDENTIFICATION OF OBS DATA

One vertical component and two horizontal components of 27 OBS data sets were recorded off eastern Taiwan in the 1995 experiment. Although not for EW9509-16 profile, OBS

stations on the other three profiles were also equipped with hydrophones to receive the compressional component of the OBS data. Data processing prior to the identification of the arrivals includes station relocation, the generation of formatted OBS data and signal enhancement (Christeson 1995; Henkart 2000). Polarization or separation of multi-component OBS data for the enhancement of the converted shear waves (Digranes et al. 1998) is not implemented because P arrivals in the vertical and compressional components appear much earlier than the converted arrivals in the horizontal components of most OBS data. To demonstrate the picking of converted arrivals, this paper presents one of the horizontal components of the OBS data from stations 8, 17, 22 and 33 and the vertical component of OBSs 8 and 33. These four OBS stations, at or near the intersection of the seismic profiles, received signals from their own profile at 2-D acquisition.

In comparison with the vertical component, the horizontal components of the OBS data show clear and first arrivals of the converted shear waves. Figure 2 shows the vertical and horizontal components of the OBS data from station 8 located on the Nanao Basin along EW9509-1. First arrivals refracting through the crust (Pg) and prominent reflections from the intra-crustal interfaces (PcP) and the Moho (PmP) Fig. 2a allow for the identification of the converted refractions through the crust (Sg) and the converted reflections from the intra-crustal interfaces (PcS) and the Moho (PmS) Fig. 2b. Except for the converted refractions through the sediment (Ss) in Fig. 2b, the sedimentary reflections of the converted shear waves cannot be

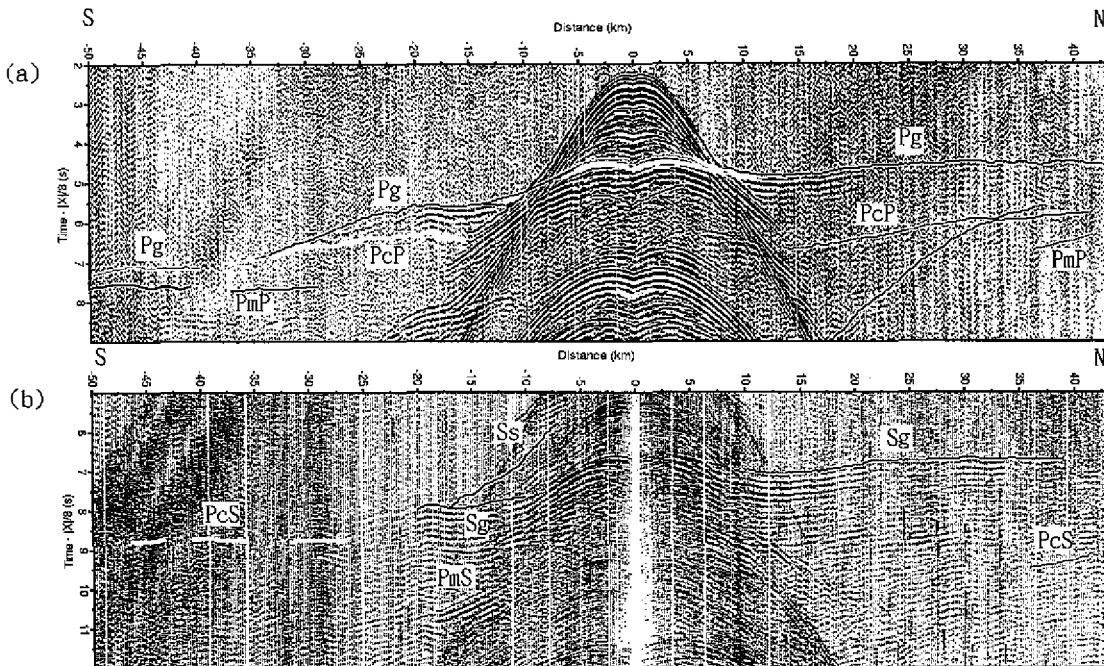


Fig. 2. (a) Vertical component and (b) horizontal component of the OBS data and picked/identified arrivals (solid lines) from OBS station 8 along EW9509-1 in the Nanao Basin.

observed from the horizontal component of OBS 8. The absence of converted reflections in the sediment is prevalent in the horizontal components of all OBS data, and this may be attributed to interference with the P-waves in the shallow depth and multiples in the fine strata.

The horizontal component of OBS 22 on the Nanao Basin along EW9509-14 (Fig. 3a) similarly displays clear first arrivals of converted refractions through the crust (Sg). Uncertainties about later arrivals of converted shear waves in the data of OBSs 22 and 8 are about 0.1 sec, which is higher than those in the data of other stations. However, these later and converted arrivals can be identified by overlapping the calculated arrivals on the horizontal components of the data. Crustal Poisson's ratios beneath the Nanao Basin are thus constrained by these identified later arrivals on the horizontal components.

First arrivals of the converted refractions through the old sediment (Ss) and the upper crust (Sg) below OBS 17 are clearly observed from the western and eastern offsets of Fig. 4a along EW9509-16, respectively. The enlarged sections of Figs. 4b and c demonstrate the picking of the converted reflections (PcS and PmS). Uncertainties about these picks on the later and converted reflections are generally less than 0.05 sec.

The similarities in the phase identification between the vertical and horizontal components of OBS 33 in Fig. 5 are less apparent than those in Fig. 2 although the first arrivals of the crustal refractions (Pg and Sg) can be readily identified from both components of Figs. 5a and b. Prominent later arrivals of the crustal reflections (PcS) are observed in the horizontal component of Fig. 5b, while the corresponding signals have not previously been picked in Fig. 5a for travel-time inversion of the P-wave model (Yang and Wang 1998). Converted shear waves in OBS 33 can be used to constrain the Poisson's ratio of the oceanic crust along EW9509-23 and beneath the Huatung Basin.

Compared with that of the first arrivals in the vertical component of the OBS data (Figs. 2a and 5a), the picking of the first converted arrivals in the horizontal component of the OBS data is more straightforward as displayed in Figs. 2b, 3a, 4a and 5b. However, most of the first arrivals are converted at the sedimentary interfaces and just beneath the OBS stations, which result in the poor constraints of the Poisson's ratios in the entire sediment. On the other hand,

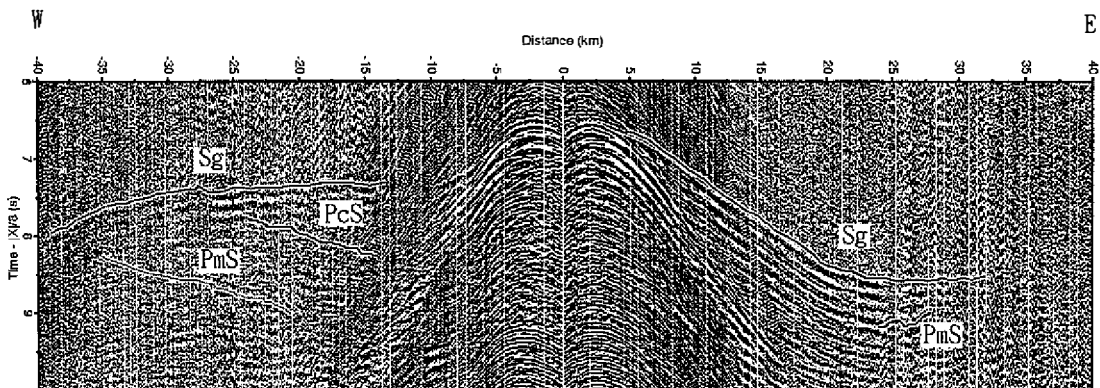
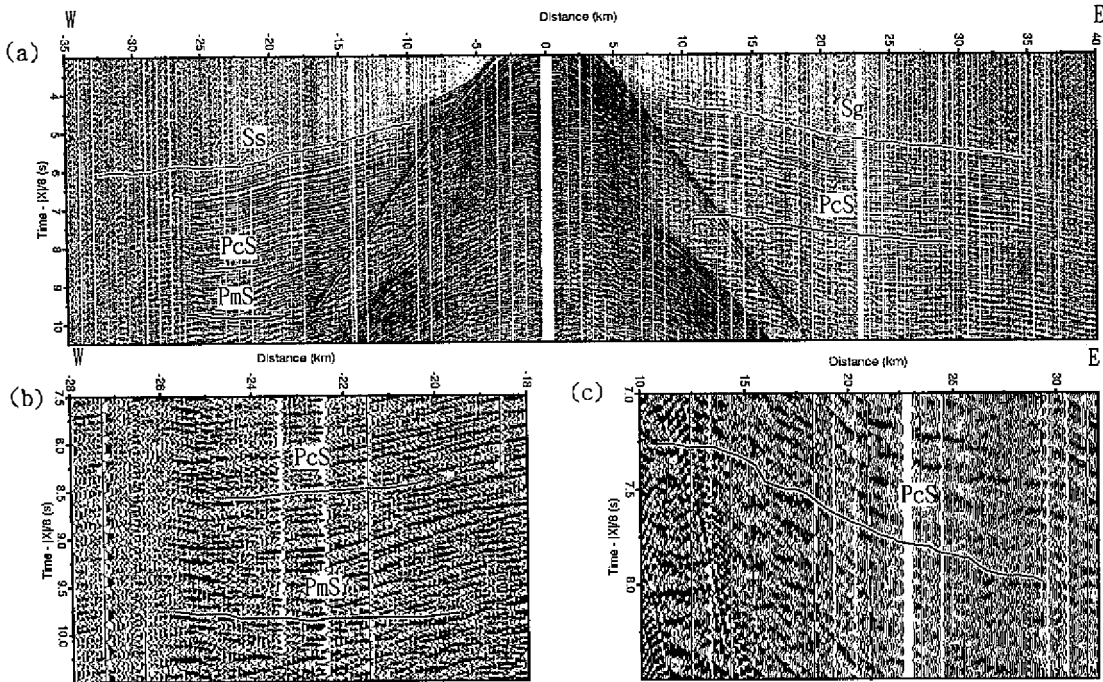


Fig. 3. (a) Horizontal component of the OBS data and picked/identified arrivals (solid lines) from OBS station 22 along EW9509-14 in the Nanao Basin.



*Fig. 4.* (a) Horizontal component of the OBS data and picked/identified arrivals (solid lines) from OBS station 17 along EW9509-16 at the eastern edge of the Hoping Basin. (b) Enlarged section at the western far-offset of (a) showing the converted arrivals reflected from the crustal interface (PcS) and the Moho (PmS). (c) Enlarged section at the eastern far-offset of (a) showing the converted arrivals reflected from the crustal interface (PcS).

the Poisson's ratios of the whole crust can be constrained by the later converted arrivals (for example, PcS and PmP) that are prominent in Fig. 5b but less obvious in Figs. 2 and 3. The uncertainties concerning the later arrivals, the identification of converted arrivals and of the converted boundaries can be clarified by superimposing the calculated arrivals on OBS data as described along with travel-time modeling in the next section.

#### 4. TRAVEL-TIME MODELING OF THE CONVERTED SHEAR WAVES

The P-wave velocity ( $V_p$ ) model has previously been determined from the travel-time inversion of MCS data and the vertical component of the OBS data in a separate study. Three sedimentary layers ( $1.51 \text{ km/sec} < V_p < 4.5 \text{ km/sec}$ ) and three crustal layers ( $4.5 \text{ km/sec} < V_p < 7.75 \text{ km/sec}$ ) in the model permit the construction of the S-wave velocity model through the use of the Poisson's ratio if the velocity interfaces of the P-wave velocity and the S-wave velocity are assumed to be the same.

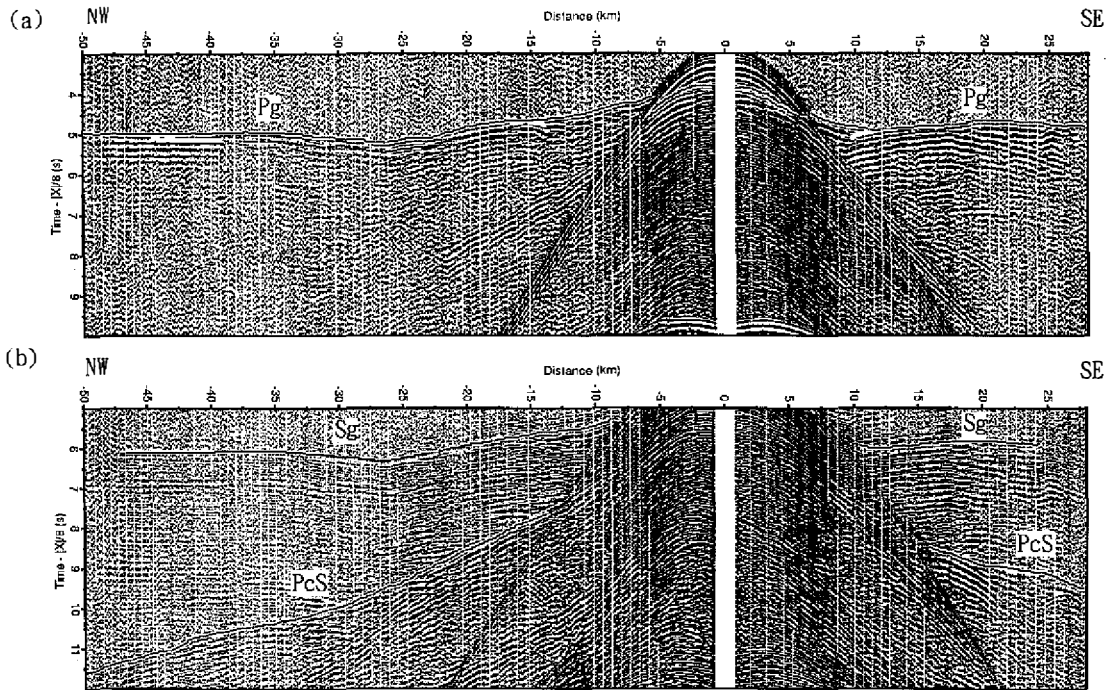


Fig. 5. (a) Vertical component and (b) horizontal component of the OBS data and picked/identified arrivals (solid lines) from OBS station 33 along EW9509-23 in the Huatung Basin. Prominent reflections from the crustal interface (PcS) can be seen from (b).

In this paper, we apply the trapezoidal profiles determined from grids of the velocity and the interface in which the Poisson's ratio is constant in each trapezoid (Zelt and Smith 1992). In the light of other OBS models (Bratt and Solomon 1984; Shaw 1994; Mjelde et al. 1995; Christensen 1996; Kodaira et al. 1996; Christeson et al. 1997), the Poisson's ratios in this study are initially set as greater than 0.4 in the upper (less consolidated) sediment ( $V_p=1.51\sim 2.2$  km/sec), as 0.3 ~ 0.45 in the lower (consolidated) sediment ( $V_p=2.2\sim 3$  km/sec), as 0.24 ~ 0.35 in the old sediment ( $V_p=3\sim 4.5$  km/sec) and the upper crust ( $V_p=4.5\sim 5.5$  km/sec), and as 0.22 ~ 0.3 in the middle and lower crusts ( $V_p=5.5\sim 7.75$  km/sec). Once the Poisson's ratio is known, S-wave velocity ( $V_s$ ) versus P-wave velocity ( $V_p$ ) can be determined from

$$\frac{V_s}{V_p} = \sqrt{\frac{0.5 - \nu}{1 - \nu}}, \quad \text{and} \quad 0 \leq \nu \leq 0.5, \quad (1)$$

where the Poisson's ratio ( $\nu$ ) and the S-wave velocity of the fluid are 0.5 and 0, respectively. In general, the  $V_s/V_p$  ratio increases as the Poisson's ratio decreases in the deeper section. By considering the P-wave velocity model and the trapezoidal model of the Poisson's ratio, the S-wave velocity model can be defined.

Since the interface of the P-S conversion is difficult to determine in advance, a layer-stripping forward modeling of the converted travel-time is implemented by adjusting the Poisson's ratios (within the ranges previously mentioned) and the converted interfaces from the upper sediment to the lower crust gradually. We find that most of the P-S conversions of the first arrivals clearly observed in our OBS data take place at the sedimentary interfaces (Kodaira et al. 1996). These first arrivals also travel as refractions with S-wave velocity within the sedimentary layers and the upper crust as illustrated by the dashed lines in Figs. 6a and 7a. Two factors may explain the P-S conversion at the sedimentary interfaces for first and refracted arrivals. First, because the distance and velocity of the shear waves traveling in the sediment and the uppermost crust are much less than their counterparts in the middle and lower crusts, the energy loss and the time delay of the converted shear waves are less and comparable to those of the primary P-waves. Secondly, due to the highly decreasing Poisson's ratios from the upper sediment to the upper crust (or increasing S-wave velocity), less energy is lost after the P-S conversions at the sedimentary interfaces (Christeson et al. 1997; Engelmark

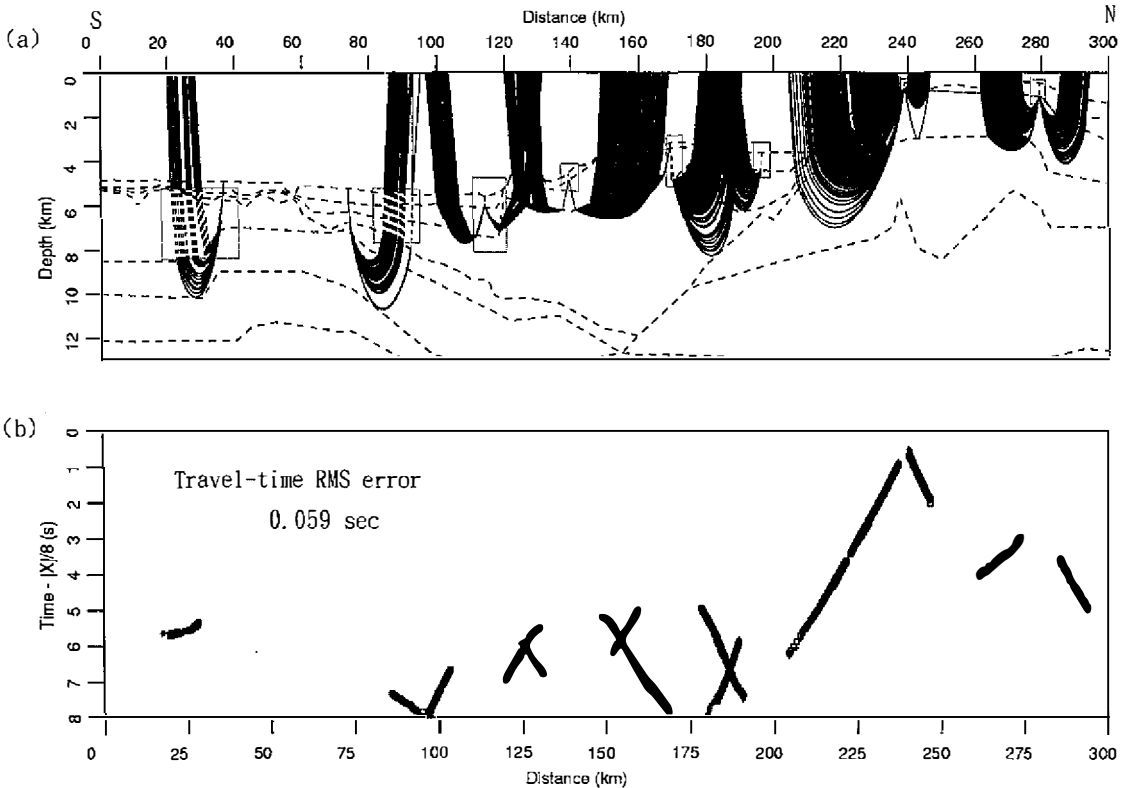
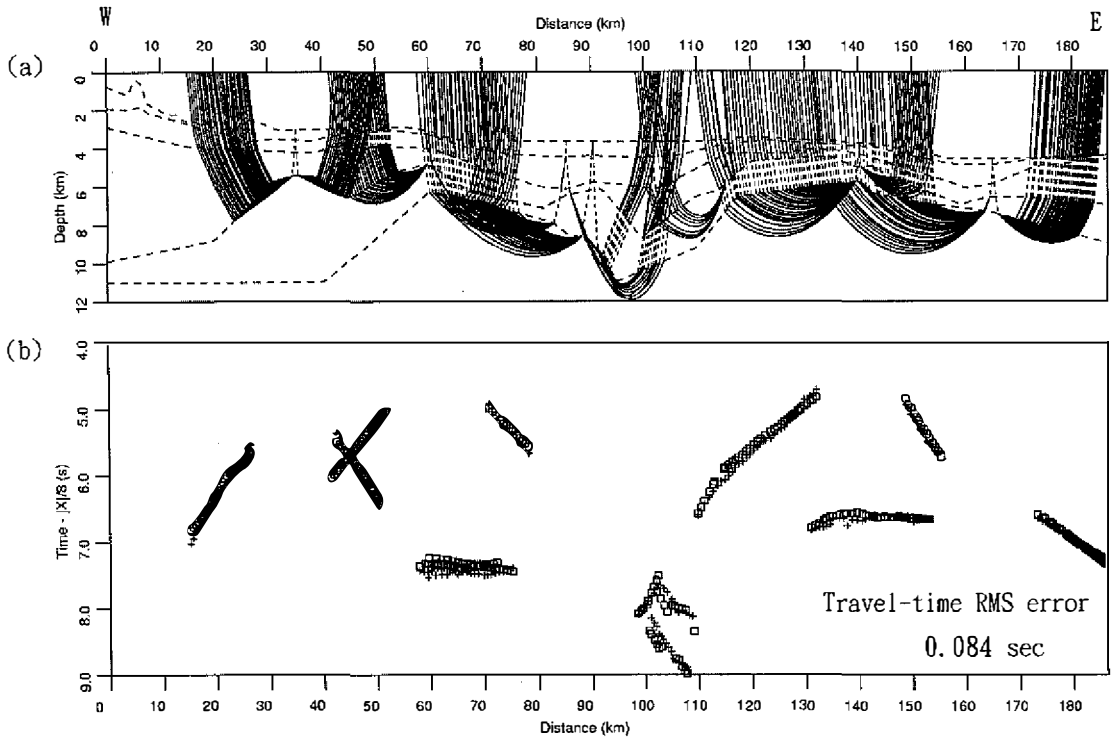


Fig. 6. (a) Ray paths of converted shear waves traveling as the first and refracted arrivals in the horizontal component of the OBS data along EW9509-1, and (b) observed (cross symbols) and predicted (small squares) arrivals of (a). Dashed rays (enclosed in small boxes) and solid rays in (a) correspond to S waves and P waves, respectively.



*Fig. 7.* (a) Ray paths of converted shear waves traveling as the first and refracted arrivals in the horizontal component of the OBS data along EW9509-14, and (b) observed (cross symbols) and predicted (small open squares) arrivals of (a). Dashed and solid rays in (a) correspond to S waves and P waves, respectively.

2000). Therefore, we take into account the converted interfaces of the sediment and the upper crust for forward modeling most of the first and clear arrivals of the converted waves in the horizontal component of the OBS data. The Poisson's ratios of the sediment below the OBS stations can then be well constrained by the clear arrivals of these converted refractions. Figures 6b and 7b demonstrate the good travel-time fits and the low RMS errors (0.059 and 0.084 sec) of the first arrivals along EW9509-1 and EW9509-14, respectively. The P-S conversion at the sedimentary interfaces for the first arrivals also suggests that reliable interfaces of the sediment in the P-wave velocity model are essential for modeling the Poisson's ratios in the sediment.

To determine the crustal Poisson's ratio, the arrivals of the P-S conversions at the crustal interfaces are similarly required for travel-time modeling. Most of the later arrivals traveling as shear waves in the horizontal components of the OBS data in this study are found as crustal reflections. The prevalence of the crustal reflections as the later arrivals can be justified from the converted and reflected rays of eight OBSs along EW9509-1 in Fig. 8a. The lack of refractions converted at the crustal interfaces may be due to the weak energy of the converted waves

traveling the long distance or because the travel time of the converted waves is longer than the recording time of the OBS data.

Complete sets of converted interfaces with various Poisson's ratios in the allowable ranges are tested in order to calculate the corresponding travel times. Calculated arrivals superimposed on the horizontal components of the OBS data then may help us to identify the proper phases of the converted signals on OBS data. Finally, we adjust the Poisson's ratios to better fit the travel times of the specified converted phases until the total RMS error of the travel times is less than 0.1 sec as shown in Fig. 8b. The maximum error of 0.1 sec is set in the travel-time modeling because it is about the maximum value of uncertainty in the travel-time picking.

### 5. POISSON'S RATIO AND ITS TECTONIC IMPLICATIONS

Unlike other OBS modeling of single Poisson's ratio in the entire layer (Mjelde et al. 1995; Kodaira et al. 1996; Digranes et al. 1998), we consider both vertical and lateral varia-

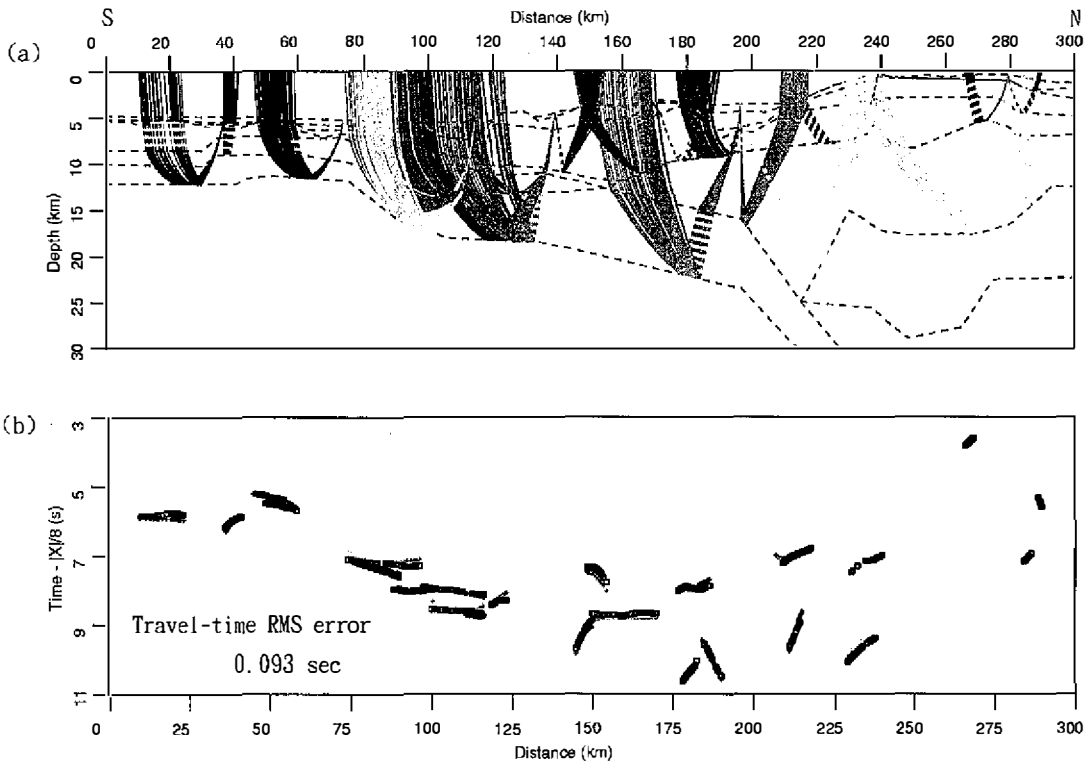


*Fig. 8.* (a) Ray paths of converted shear waves traveling as the later and reflected arrivals in the horizontal component of the OBS data along EW9509-1 and (b) observed (cross symbols) and predicted (small open squares) arrivals of (a). Dashed and solid rays in (a) correspond to S waves and P waves, respectively.

tions of the Poisson's ratios in four OBS profiles off eastern Taiwan. Constraints on the Poisson's ratios within the trapezoidal profiles are evaluated from the coverage of shear rays since the P-wave alone does not constrain the Poisson's ratio. In the following, for each of the trapezoidal models in the OBS profiles (EW9509-1, EW9509-14, EW9509-16 and EW9509-23), we first present the coverage of shear rays (dashed lines) and the associated travel-time fit, then go on to describe the anomalous Poisson's ratios (shaded trapezoids) and finally discuss their tectonic implications.

The reflected and converted rays in the EW9509-1 profile are displayed in Fig. 8a. The multiple crossing of shear rays (dashed lines) through the oceanic crust south of the accretionary prism, the northern portion of the accretionary prism and the southern portion of the upper continental crust demonstrate good constraints of the Poisson's ratios. However, from the single coverage of the shear ray in Fig. 8a, the Poisson's ratios in the subducting slab north of the accretionary prism and in most of the Ryukyu Arc basement are less constrained. The travel-time fits of the converted shear waves in the EW9509-1 profile of Fig. 8b are generally good with a travel-time RMS error of 0.093 sec. Owing to the lower sediment in the trapezoidal model of EW9509-1 in Fig. 9, the Poisson's ratio (0.31 in the shaded trapezoids) of the Ryukyu Trench and the Nanao Basin is lower than the average Poisson's ratio (0.32 in the triangular bracket) of the lower sediment. The low Poisson's ratio of the lower sediment may imply consolidation and subsidence in the trench and the forearc basin. From crustal structures

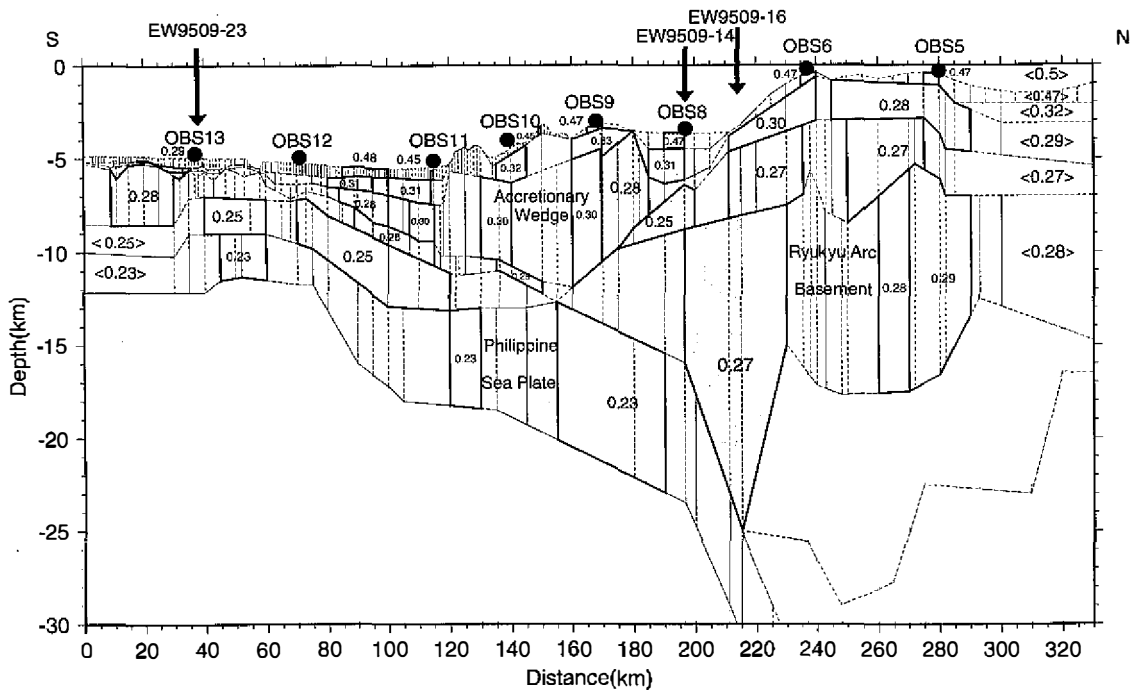


Fig. 9. Poisson's ratios in the trapezoidal model (dashed lines) of EW9509-1. Value in the triangular bracket is the average Poisson's ratio of the corresponding layer.

beneath the Nanao Basin, we find sharp contrasts of the Poisson's ratios in the Yaeyama accretionary prism (0.28), the Ryukyu Arc basement (0.25~0.27) and the subducting slab of the PSP (0.23) in Fig. 9. These differences in the Poisson's ratios confirm the variations in the tectonic provinces of the accretionary prism, the continental and oceanic crusts in the plate boundaries. The anomalously low Poisson's ratios beneath the Nanao Basin are also identified from the shaded trapezoids in Fig. 9. The Poisson's ratio (0.28) of the northern Yaeyama accretionary prism (below OBSs 8 and 9) is the lowest in the accretionary prism (0.3 of the Poisson's ratio), and the Poisson's ratio (0.25~0.27) of the Ryukyu Arc basement beneath the Nanao Basin (below OBSs 6~9) is lower than those north of the Nanao Basin (0.27~0.29). We infer that these anomalously low Poisson's ratios may have resulted from fractures from the forearc compression of the Ryukyu Arc by the northward subduction of the PSP.

Full coverage of the shear rays (dashed lines) but with only one crossing in the crust is shown in the reflected rays along EW9509-14 of Fig. 10a. Good fits of the converted and reflected arrivals from seven OBS stations with an RMS error of 0.06 sec are also demonstrated in Fig. 10b. Similar to the low Poisson's ratio of the Nanao Basin along EW9509-1 in Fig. 9, the Poisson's ratio (0.31) of the lower sediment in the Nanao Basin (below OBSs 22

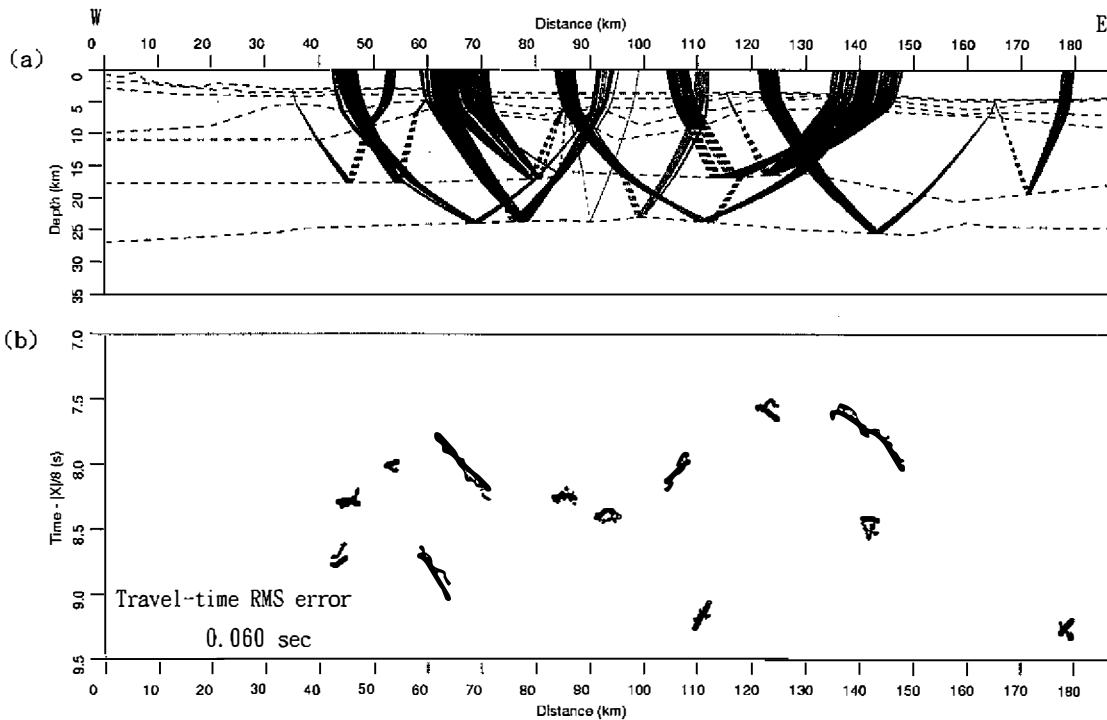


Fig. 10. (a) Ray paths of converted shear waves traveling as the later and reflected arrivals in the horizontal component of the OBS data along EW9509-14, and (b) observed (cross symbols) and predicted (small squares) arrivals of (a). Dashed and solid rays in (a) correspond to S waves and P waves, respectively.

and 23) is the lowest of all Poisson's ratios (0.33~0.35) of the lower sediment in the rest of the EW9509-14 profile (Fig. 11). This low Poisson's ratio may also be attributed to more consolidated sediments and thus good sedimentary subsidence in the Nanao Basin. Crustal Poisson's ratios in Fig. 11 also show a sharp contrast of the Poisson's ratios (from 0.25 eastward increasing to 0.32 in the shaded trapezoids) in the upper crust beneath the eastern portion of the Nanao Basin (below OBSs 23 and 24) and anomalously high Poisson's ratios (0.27 for the middle crust and 0.24 for the lower crust in the shaded trapezoids) in the crust beneath the Nanao Basin (below OBSs 22~24). These anomalously high Poisson's ratios in the crust beneath the Nanao Basin may reportedly imply either fluid-filled fractures (Mjelde et al. 1995) or less fractured rocks (Shaw 1994). However, since the Luzon Arc and Ryukyu Arc might have collided below OBSs 20 and 21 (Wang and Chiang 1998) and the Gagua Ridge may have subducted northward below OBSs 24 and 25 (Schnurle et al. 1998), the interpretation that there are fluid-filled micro-cracks beneath the Nanao Basin likely seems the most reasonable.

The converted shear rays along EW9509-16 in Fig. 12a show that the coverage of shear rays (and thus constraints of the Poisson's ratios) in the sediment and in the crust is restricted below OBS stations and OBSs 16~18, respectively. The travel-time fits of all arrivals except for the easternmost arrivals are generally good with a total RMS error of 0.078 sec (Fig. 12b). As shown in Fig. 13, the Poisson's ratios of the sediment (0.43~0.45) in the northern edge of the Nanao Basin (below OBSs 16 and 17) are higher than the Poisson's ratios of the sediment

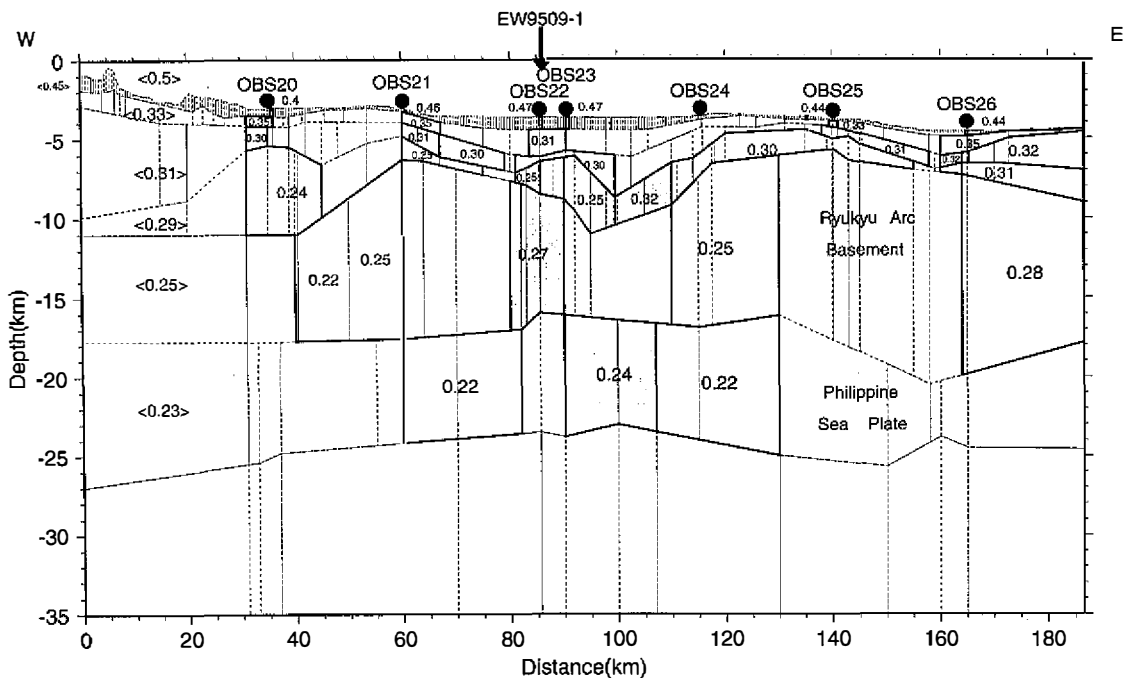


Fig. 11. Poisson's ratios in the trapezoidal model (dashed lines) of EW9509-14. Value in the triangular bracket is the average Poisson's ratio of the corresponding layer.

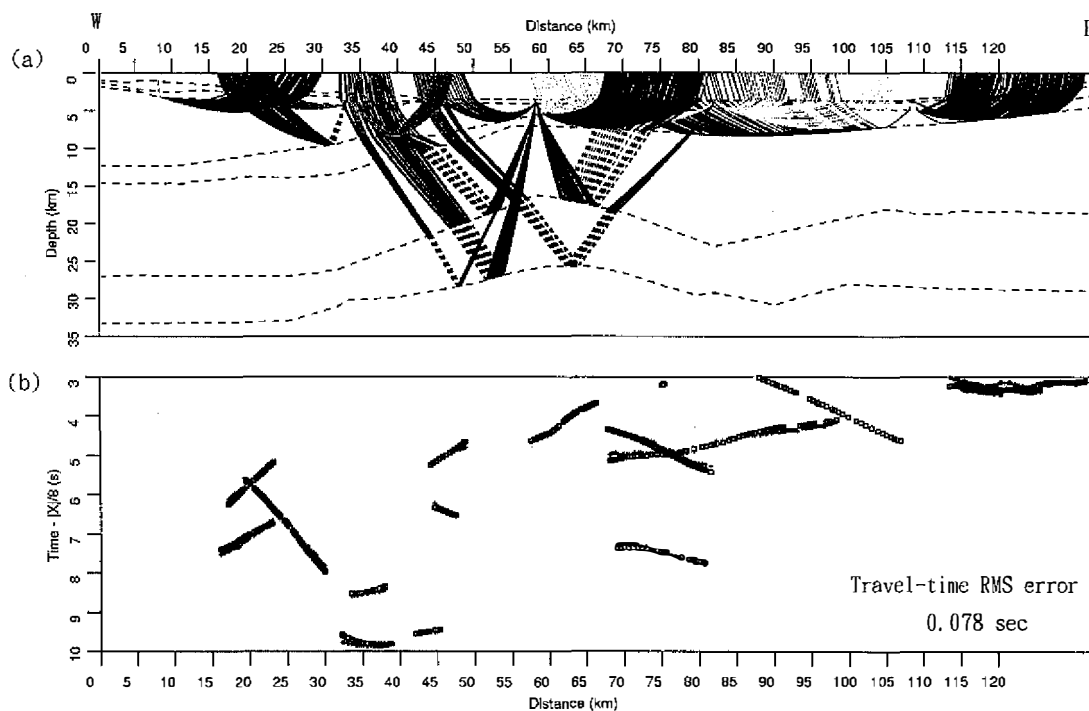


Fig. 12. (a) Ray paths of converted shear waves traveling along EW9509-16, and (b) observed (cross symbols) and predicted (small open squares) arrivals of (a). Dashed and solid rays in (a) correspond to S waves and P waves, respectively.

(0.41) in the rest of the EW9509-16 profile. Regardless of the low Poisson's ratio in the central Nanao Basin along EW9509-1 and EW9509-14, the high Poisson's ratio in the northern edge of the Nanao Basin may imply less consolidated sediments. Anomalously high Poisson's ratios (0.27~0.29) of the middle crust beneath the northern edge of the Nanao Basin (below OBSs 16~17) are also observed in Fig. 13. The high Poisson's ratio of the crust along EW9509-16 is consistent with that along EW9509-1 and may also be a result of fluid-filled fractures caused by the northward movement of the Luzon Arc and the Gauga Ridge.

Full and multiple coverage of shear rays along EW9509-23 with a travel-time RMS error of 0.07 sec is displayed in Fig. 14. This profile has the best constraint on the Poisson's ratio compared with the other three profiles because the quality of the horizontal components of the OBS data is generally high (Fig. 5b). A decrease in the Poisson's ratios northwestward along EW9509-23 in Fig. 15 is consistent with an increase in thickness of the crust northwestward. Furthermore, sharp contrasts (0.03~0.06) of the Poisson's ratios below OBSs 30 and 31 can be observed in Fig. 15. We infer that the northwestern portion (shaded area) of EW9509-23 is fractured and may belong to the collision front of the Luzon Arc and the EP continent.

The average Poisson's ratios (values in the triangular brackets) of each layer in the four trapezoidal profiles (Figs. 9, 11, 13 and 15) generally decrease in the deeper layers as sug-

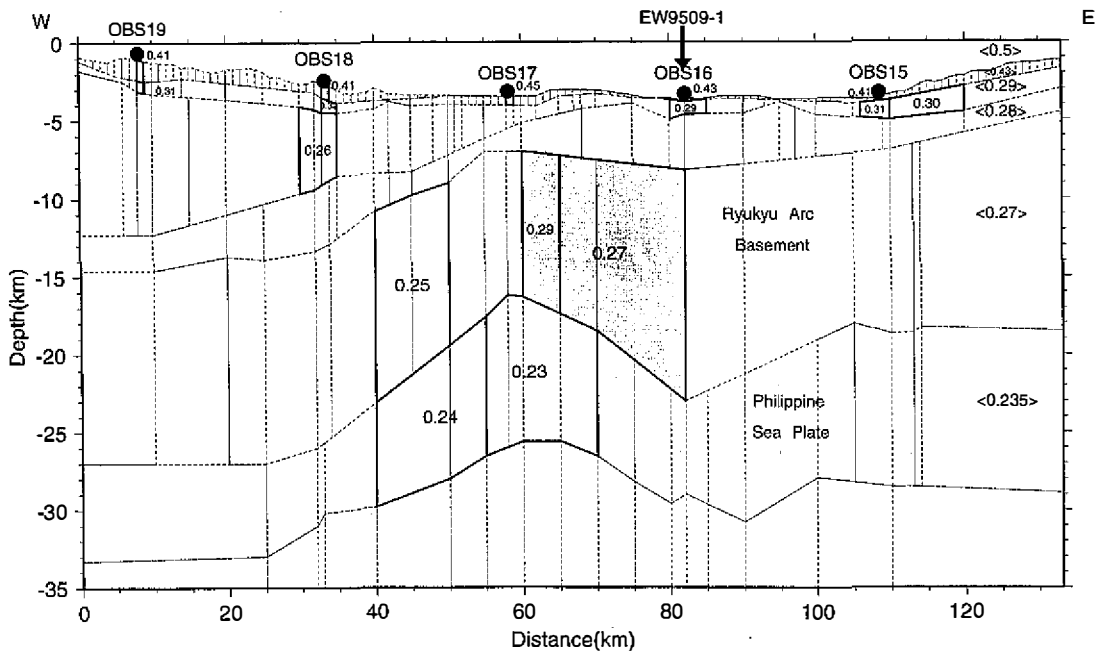
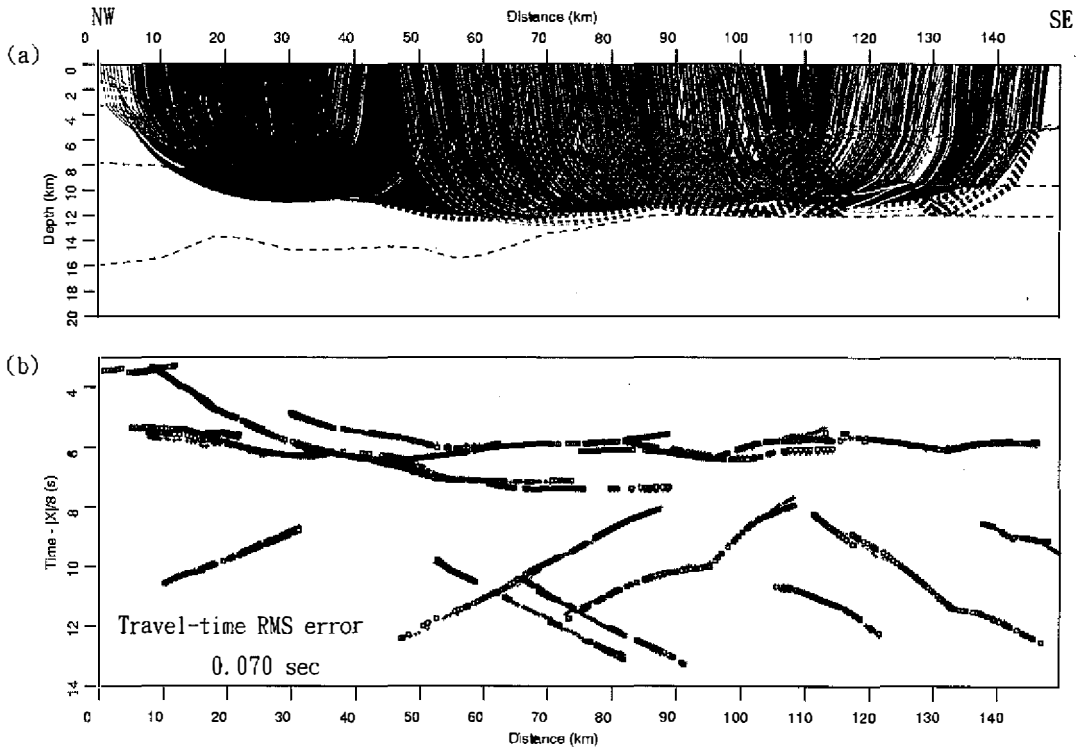


Fig. 13. Poisson's ratios in the trapezoidal model (dashed lines) of EW9509-16. Value in the triangular bracket is the average Poisson's ratio of the corresponding layer.

gested by the initial models. For example, the average Poisson's ratios of the lower, upper and old sediments are 0.43~0.47, 0.29~0.33 and 0.29~0.31, respectively, whereas those of the upper and lower crusts of the continent are 0.27~0.29 and 0.25~0.28, respectively. Variations of these average Poisson's ratios from all of the profiles are generally less than 0.04 within each layer. In contrast, the average Poisson's ratio of the oceanic crust varies significantly among the different profiles. The average Poisson's ratio in the middle and lower crusts of the PSP along all profiles other than EW9509-23 are 0.25 and 0.22~0.24, respectively. The low Poisson's ratio of the oceanic crust in the Huatung Basin and along EW9509-1 may be affected by the Taitung Canyon fault zone from the Gagua Ridge (Hsu et al. 1998; Kao et al. 2000), whereas those beneath the Nanao Basin may be inferred from the northward movement of the Luzon Arc and the Gagua Ridge as mentioned before. However, along EW9509-23, the average Poisson's ratio of 0.3 in the oceanic crust is much higher than those along other profiles. Velocity anisotropy of the shear waves (Mjelde et al. 1995) beneath the Huatung Basin may be associated with the difference of the Poisson's ratios in the oceanic crust along EW9509-1 and EW9509-23.

## 6. CONCLUSIONS

In this study, most of the first arrivals in the horizontal components of the OBS data are



*Fig. 14.* (a) Ray paths of converted shear waves traveling along EW9509-23, and (b) observed (cross symbols) and predicted (small open squares) arrivals of (a). Dashed and solid rays in (a) correspond to S waves and P waves, respectively.

clearly identified as converted refractions traveling as shear waves in the sediment and in the upper crust. On the other hand, we interpret most of the later arrivals in the horizontal components of the OBS data as converted reflections for modeling the crustal Poisson's ratios. Layer-stripping forward modeling of converted shear arrivals generates four trapezoidal profiles of the Poisson's ratio. The results are applied to investigate sedimentary subsidence, to elaborate structural boundaries from tectonic settings and to infer fractures and fluid intrusions from tectonic motions.

In this paper, sedimentary subsidence in the Nanao Basin and in the Ryukyu Trench is inferred from low Poisson's ratio (0.31) of the lower sediment. The tectonic boundaries among the accretionary prism, the continental crust and the oceanic slab in the Ryukyu forearc region are further identified from differences of the Poisson's ratios which are 0.28~0.3, 0.25~0.29 and 0.23~0.33, respectively. As for tectonic motions beneath the Nanao Basin, since the northward subduction of the PSP results in forearc compression and a fracture zone near the Nanao Basin, relatively low Poisson's ratios in the northern portion of the Yaeyama accretionary prism (0.28) and in the southern portion of the Ryukyu Arc basement (0.25) are found along EW9509-1. Furthermore, since the northward movement of the Luzon Arc and the Gauga

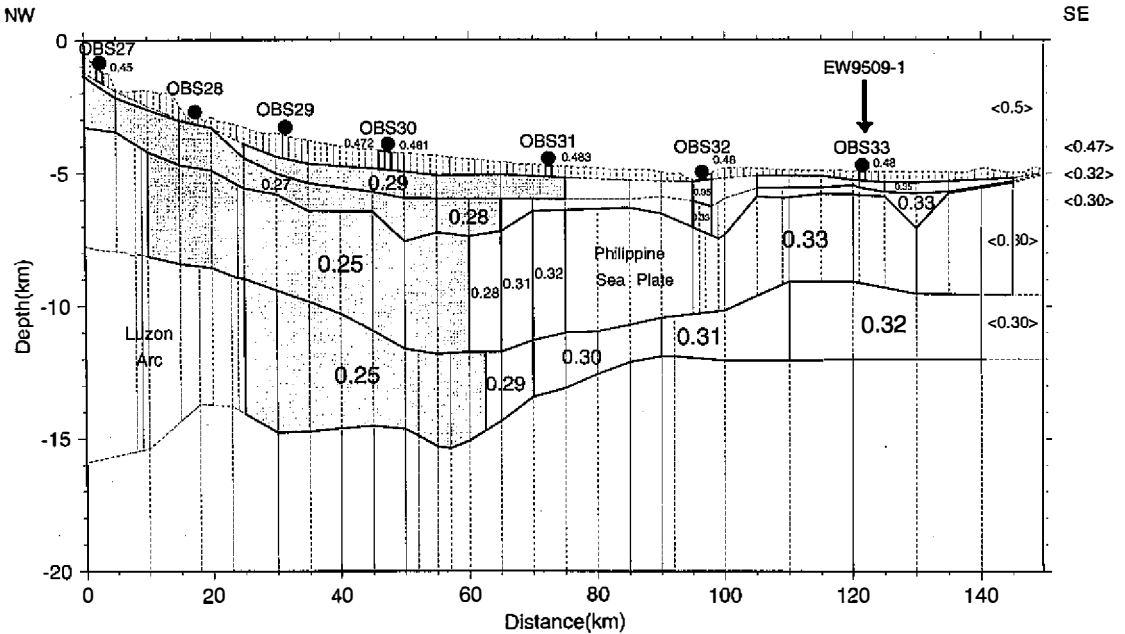


Fig. 15. Poisson's ratios in the trapezoidal model (dashed lines) of EW9509-23. Value in the triangular bracket is the average Poisson's ratio of the corresponding layer.

Ridge have led to fluid-filled fractures beneath the Nanao Basin, the anomalously high Poisson's ratios of the Ryukyu Arc basement (0.27~0.29) beneath the Nanao Basin are imaged along EW9509-14 and EW9509-16. For tectonic motions beneath the Huatung Basin, the arc-continent collision along EW9509-23 may be responsible for an increase in thickness and a decrease in the Poisson's ratio of the PSP northwestward. The sharp contrasts (0.03~0.06) of the Poisson's ratios and the abrupt change (about 3 km) in the crustal thickness between OBSs 30 and 31 may also be related to the arc-continent collision.

**Acknowledgements** We appreciate Professor Char-Shine Liu's thorough and constructive review of this paper. We also thank two anonymous reviewers for their efforts to improve this paper. This work has been supported by the National Science Council of Taiwan under grants NSC 86-2117-M019-002-ODP, NSC 87-2611-M019-011-ODP and NSC 88-2611-M019-014-ODP.

## REFERENCES

- Bratt, S. R., and S. C. Solomon, 1984: Compressional and shear wave structure of the East Pacific Rise at 11°20' N: constraints from three-component ocean bottom seismometer data. *J. Geophys. Res.*, **89**, 6095-6110.
- Cheng, W. B., C. S. Wang, and C. T. Shyu, 1996: Crustal structure of the northeastern Taiwan

- area from seismic refraction data and its tectonic implications. *TAO*, **7**, 467-487.
- Christensen, N., 1996: Poisson's ratio and crustal seismology. *J. Geophys. Res.*, **101**, 3139-3156.
- Christeson, G., 1995: OBSTOOL, software for processing UTIG OBS data. University of Texas, Institute for Geophysics, Technical Report No. 134, pp. 27.
- Christeson, G. L., P. R. Shaw, and J. D. Garmany, 1997: Shear and compressional wave structure of the East Pacific Rise, 90-100 N. *J. Geophys. Res.*, **102**, 7821-7835.
- Digranes, P., R. Mjelde, S. Kodaira, H. Shimamura, T. Kanazawa, H. Shiobara, and E. W. Berg, 1998: A regional shear-wave velocity model in the central Voring Basin, N. Norway, using three-component ocean bottom seismographs. *Tectonophysics*, **293**, 157-174.
- Engelmark, F., 2000: Using converted shear waves to image reservoirs with low-impedance contrast. *The Leading Edge*, **19**, 600-603.
- Hagen, R. A., F. K. Duennebieer, and V. Hsu, 1988: A seismic refraction study of the crustal structure in the active seismic zone east of Taiwan. *J. Geophys. Res.*, **93**, 4785-4796.
- Henkart, P., 2000: SIOSEIS users' manual, version 2000.2. Scripps Institution of Oceanography, University of California, San Diego.
- Holbrook, W. S., D. Gajewski, A. Krammer, and C. Prodehl, 1988: An interpretation of wide-angle compressional and shear wave data in southwest Germany: Poisson's ratio and petrological implications. *J. Geophys. Res.*, **93**, 12081-12106.
- Hsu, S. K., C. S. Liu, C. T. Shyu, S. Y. Liu, J. C. Sibuet, S. Lallemand, C. S. Wang, and D. Reed, 1998: New gravity and magnetic anomaly maps in the Taiwan-Luzon region and their preliminary interpretation. *TAO*, **9**, 509-532.
- Hsu, S. K., 2001: Subduction/collision complexities in the Taiwan-Ryukyu junction area: tectonics of the northwestern corner of the Philippine Sea Plate. *TAO*, **12**, 209-230.
- Iwasaki, T., M. A. Sellevoll, T. Kanazawa, T. Veggeland, and H. Shimamura, 1994: Seismic refraction crustal study along the Sognefjord, south-west Norway, employing ocean-bottom seismometers. *Geophys. J. Int.*, **119**, 791-808.
- Kao, H., G. C. Huang, and C. S. Liu, 2000: Transition from oblique subduction to collision in the northern Luzon Arc: Constraints from bathymetry and seismic observations. *J. Geophys. Res.*, **105**, 3059-3079.
- Kodaira, S., M. Bellenberg, T. Iwasaki, T. Kanazawa, H. B. Hirschleber, and H. Shimamura, 1996:  $V_p/V_s$  ratio structure of the Lofoten continental margin, northern Norway, and its geological implications. *Geophys. J. Int.*, **124**, 724-720.
- Liu, C. S., P. Schnurle, S. E. Lallemand, and D. L., Reed, 1997: TAICRUST and deep seismic imaging of western end of Ryukyu arc-trench system. In: K. Fujioka (Ed.), Deep Sea Research in Subduction Zones, Spreading Centers and Backarc Basins, JAMSTEC Journal of Deep Sea Res., 39-45.
- McIntosh, K. D., and Y. Nakamura, 1998: Crustal structure beneath the Nanao forearc basin from TAICRUST MCS/OBS Line 14. *TAO*, **9**, 345-362.
- Mjelde, R., M. A. Sellevoll, H. Shimamura, T. Iwasaki, and T. Kanazawa, 1995: S-wave anisotropy off Lofoten, Norway, indicative of fluids in the lower continental crust? *Geophys. J. Int.*, **120**, 87-96.

- Schnurle, P., C. S. Liu, S. E. Lallemand, and D. L. Reed, 1998: Structural insight into the south Ryukyu margin: Effects of the subducting Gagua Ridge. *Tectonophysics*, **288**, 237-250.
- Shaw, P. R., 1994: Age variations of oceanic crust Poisson's ratio: inversion and a porosity evolution model. *J. Geophys. Res.*, **99**, 3057-3066.
- Tinivella, U., and F. Accaino, 2000: Compressional velocity structure and Poisson's ratio in marine sediments with gas hydrate and free gas by inversion of reflected and refracted seismic data (South Shetland Islands, Antarctica). *Marine Geology*, **164**, 13-27.
- Wang, T. K., 1997: Shear wave structures of the crust offshore eastern Taiwan. *Chinese Geophysical Symposium*, 235-239.
- Wang, T. K., S. F. Lin, W. N. Wu, C. H. Pan, and C. S. Liu, 1998: Shear and compressional wave structures explored by ocean bottom seismometers offshore eastern Taiwan. *EOS*, **79**, W75.
- Wang, T. K., and C. H. Chiang, 1998: Imaging of arc-arc collision in the Ryukyu forearc region offshore Hualien from TAICRUST OBS Line 16. *TAO*, **9**, 329-344.
- Wang, T. K., K. D. McIntosh, Y. Nakamura, C. S. Liu, and H. W. Chen, 2001: Velocity-interface structure of the southwestern Ryukyu subduction zone from EW9509-1 OBS/MCS data. Submitted to *J. Geophys. Res.* .
- Yang, Y. S., and T. K. Wang, 1998: Crustal velocity variation of the western Philippine Sea Plate from TAICRUST OBS/MCS Line 23. *TAO*, **9**, 379-393.
- Zelt, C. A., and R. B. Smith, 1992: Seismic travelttime inversion for 2-D crustal velocity structure. *Geophys. J. Int.*, **108**, 16-34.